Stability and Phase Formation in the $(Li/Na)_6C_{60}$–H Systems Studied by Neutron Scattering

Sabrina Sartori,[a,*] Matylda N. Guzik,[a] Kenneth D. Knudsen,[b] Magnus H. Sørby,[b] Joseph A. Teprovich Jr.,[c] Ragaiy Zidan,[d] Bjørn C. Hauback[b]

[a] *Department of Technology Systems, University of Oslo, P.O. Box 70, NO-2027 Kjeller, Norway*

[b] *Department for Neutron Materials Characterization, Institute for Energy Technology, P.O. Box 40, NO-2027 Kjeller, Norway*

[c] *Department of Chemistry and Biochemistry, California State University Northridge, 18111 Nordhoff St., Northridge, CA 91330, USA*

[d] *Savannah River National Laboratory, Aiken, SC 29808, USA*

*Corresponding author: e-mail: sabrina.sartori@its.uio.no

Abstract

Small-angle neutron scattering (SANS) combined with powder neutron diffraction (PND) were employed to study phase formation upon absorption/desorption of hydrogen gas in Li- and Na-intercalated fullerides. The comparative system analysis, addressing changes in the sample phase compositions and morphology of powders, revealed higher degree of complexity in the Na-based samples. Results also showed that disappearance of the crystalline lithium/sodium hydride during desorption was accompanied by an increased surface roughness in both systems, most likely due to formation of a local surface strain. Furthermore, increased specific internal surface of the studied materials upon subsequent deuterium absorption/desorption cycles was demonstrated. This could indicate moderate fracturing of crystallites.

1. Introduction

Unusual physical properties of alkali and alkaline earth metal intercalated fullerides have resulted in extended studies of this group of compounds.[1-9] More recently, light metal-based systems, in particular Li- and Na-incorporating fullerenes, have gained additional interest due to

their properties suitable for energy storage applications, e. g. for batteries[10-13] and hydrogen storage.[14-29] Correlation between structural properties of Na- and Li-based fullerides and their chemical and physical characteristics have been studied extensively by many techniques, including powder X-ray and neutron diffraction (PXD and PND, respectively),[15, 17, 19-26, 30-33] nuclear magnetic resonance (NMR),[26, 28, 34] differential scanning calorimetry (DSC),[20, 22, 26, 29] infrared spectroscopy (IR).[17, 19, 25-26] However, the published results still lead to contradictory conclusions about sample phase compositions and metal(M):C_{60} ratios. Comprehensive diffraction studies have been carried out for both Li_xC_{60} and Na_xC_{60} systems in a wide range of metal atom concentrations.[9, 14, 19-26, 28, 30-33] The results demonstrate variations in structure types and symmetries among the formed intercalated fullerides, which were likely to originate from the applied synthesis methods and/or the M: C_{60} ratio.

The small size of Li ions, with respect to a relatively large free volume of fullerenes, allowed for synthesis of a broad family of Li_xC_{60} compounds.[15, 19-20, 23, 26, 35-37] Li_4C_{60} is one of the most studied compositions. It was reported to crystallize with a monoclinic (*I*2/*m*) polymeric structure at room temperature (RT) that transformed to a monomeric face-centered cubic (*fcc*) symmetry at higher temperatures.[36-38] Other Li_xC_{60} systems, with a higher x (≥ 6), formed monomeric phases with Li clusters inside the fullerene voids.[23, 39-40] Li_6C_{60} forms the *fcc* structure with a small contraction of the unit cell volume, as compared to the pristine C_{60}.[15, 21, 26, 34] The reported Li_xC_{60}, with x = 12 and 28, crystallized at RT as a cubic or pseudo-cubic Li_xC_{60} phase with small Li clusters residing at the available interstitial sites.[19-20, 23, 35]

$Na_{1.3}C_{60}$ was reported to form a simple primitive unit cell (*Pa*-3) at 300 K, which transformed to *Fm*-3*m* above 325 K.[32] Na_2C_{60} was shown to crystallize with the *fcc* (*Fm*-3*m*) unit cell at 290 K, in which Na atoms occupied the tetrahedral sites of the fullerene sublattice.[24, 30, 41] Na_3C_{60} also has the *fcc* (*Fm*-3*m*) symmetry at 300 K but Na atoms occupy both tetrahedral and octahedral interstitial sites.[24, 30] This compound disproportionates below 250 K into two *fcc* phases with unit cell parameters corresponding to those of Na_2C_{60} and Na_6C_{60}, respectively. Na_3C_{60} is also anticipated to crystalize with a low-symmetry (tri- or monoclinic) structure or as a mixture of Na_xC_{60} phases with various Na:C_{60} ratios.[41] Na_4C_{60} forms a 2D polymerized structure with a body-centered monoclinic (*bcm*) unit cell (*I*2/*m*) that can transform reversibly to a monomeric body-centered tetragonal (*bct*) phase above 500 K.[33, 42-43] However, in another study,

Na_4C_{60} was shown to crystallize as a single phase with a hexagonal close-packed (*hcp*) atom arrangement.[24] The Na_6C_{60} system was reported to adopt the *fcc* unit cell (*Fm*-3*m*), in which single Na atoms centered at the tetrahedral interstitial sites and Na_4 clusters were distributed over octahedral ones.[15, 17, 30] Na_xC_{60} with a higher Na:C_{60} ratio, x = 7.2, 9, 9.7, 11 and 12, were found to form a *fcc* phase (*Fm*-3) with Na clusters at octahedral sites and single metal atom occupancy at the tetrahedral ones.[31] Later studies demonstrated that $Na_{7.7}C_{60}$ and $Na_{10}C_{60}$ could also crystallize with the *fcc* (*Fm*-3) atomic arrangement[20, 25] and powder diffraction data for Na_xC_{60}, with x = 9 and 11, were successfully indexed with a hexagonal unit cell.[24]

Presence of alkali clusters inside the C_{60} appears to be fundamental for the hydrogen sorption properties of the Li- and Na-based fullerides.[15-17, 19-22, 25-26, 29, 44] Their formation allows for the dissociation of H_2 and migration of hydrogen atoms inside the C_{60} crystal lattice. This reversible process improves kinetics and lowers hydrogenation temperature of the obtained compounds as compared to the pristine C_{60}. Hydrogenation studies for the Li_xC_{60}-H_y and Na_xC_{60}-H_y systems showed that while the former could absorb up to 5 wt.% of H_2, the latter stored 4 wt.% of hydrogen.[15, 19, 25-26, 44] Although the Na-intercalated fulleride stores less hydrogen in terms of gravimetric capacity, they enable the formation of extremely hydrogenated C_{60}. Recent mass spectrometry and fluorescence experiments are consistent with the formation of $C_{60}H_{60}$ with Na intercalation, while Li intercalation was only able to achieve up to $C_{60}H_{48}$.[45-46] However, the high stability of both hydrogenated systems allowed for the H_2 desorption only at 673 K and 823 K for the Li- and Na-based fullerides, respectively.

Hydrogen-induced phase transformations have only been studied for a limited number of compositions. The reversible hydrogen-induced *fcc–bcc* (body-centered cubic) phase transition was demonstrated for Li_6C_{60} and associated with a partial de/reintercalation of Li upon H_2 absorption and desorption, respectively.[15, 21, 26, 34] For $Li_{12-x}C_{60}$, PXD and PND data confirmed formation of a *fcc* $Li_{12-x}C_{60}$-H_y phase at 493 K and 190 bar of H_2.[19] Furthermore, the migration of Li atoms from the fulleride structure and crystallization of LiH were also observed. The same system at higher temperature (623 K) and lower gas pressure (100 bar) went through a phase transition, which led to crystallization of the *bcc* $Li_{12-x}C_{60}$-H_y phase and LiH. Later, the same research group reported on the hydrogenation of $Li_{12}C_{60}$ at 623 K and 180 bar of H_2 and again demonstrated the formation of *bcc* $Li_{12-x}C_{60}$-H_y and LiH.[20] The latter disappeared during the

dehydrogenation process, which again was associated with the reintercalation of Li atoms into the fulleride crystal structure.

Na_6C_{60}-H_y has been claimed to store hydrogen reversibly at 623 K and under 100 bar of H_2.[15, 17] Upon hydrogenation a phase transition occurred, in which the *fcc* structure of the H-free Na_6C_{60} transformed into *bcc* (*Im*-3).[15, 17] In another study, cubic $Na_{10-x}C_{60}$ was shown to form the hydrogenated *fcc* structure at 423 K and under 200 bar of H_2.[25] The hydrogenation process was associated with deintercalation of Na atoms from the fulleride lattice and formation of NaH. At higher temperatures (673 K) hydrogen is desorbed from both phases ($Na_{10-x}C_{60}$-H_y and NaH), thus resulting in reintercalation of Na atoms into the fulleride. The H-free $Na_{10-x}C_{60}$ retained the original *fcc* symmetry with a unit cell size similar to that of $Na_{10}C_{60}$.

Very recent data showed successful synthesis of compounds with a nominal composition $Na_xLi_{6-x}C_{60}$, x = 0–6[22, 28] and $Na_xLi_{12-x}C_{60}$, x = 1–6.[27] As formed phases crystallized with the *fcc* symmetry and demonstrated ability to the reversible storage of hydrogen. However, the $Na_xLi_{6-x}C_{60}$ family showed better sorption performance than $Na_xLi_{12-x}C_{60}$.

In order to bring a new perspective on H-induced changes in Li- and Na-based fullerides we applied for the first time small-angle neutron scattering (SANS) combined with powder neutron diffraction (PND). SANS is important to follow nanoscale changes occurring in these metal intercalated fullerides under varying conditions of temperature and deuterium loading. The technique is sensitive to structural rearrangements on a scale from ca. 1 to 100 nm, given that the changes occurring produce a local variation in either the mass density or the relative composition of the material. Modifications in surface structure (of particles/crystallites) are also probed, via a fractal dimension parameter and the specific surface (area per volume or gram). Thus, the information obtained by small angle scattering is important to correlate structural changes on the atomic scale with modifications occurring on longer scales, as probed with diffraction. Such information is highly relevant to get a deeper understanding of the mechanisms behind hydrogen absorption and desorption in these materials.

2. Materials and methods

Na- and Li-based fullerides were synthesized from C_{60} and ^{7}LiD/NaD powders stirred in THF. The isotopes ^{7}Li and ^{2}H (D) were used for the sample preparation in order to obtain low

absorption and adequate signal/noise ratio in the neutron experiments. The M:C_{60} ratio was 6:1 for both systems. The subsequent mixtures were transferred into quartz tubes and heated under vacuum at 773 K (Li) and 743 K (Na), thus resulting in release of THF and desorption of D_2. In order to obtain deuterium containing powders, the samples were kept under 100 bars of D_2 gas at elevated temperatures for 8 hours; Li_6C_{60} at 623 K and Na_6C_{60} first at 523 K and then at 623 K. The Li-based sample was desorbed again at 803 K. To simplify sample identification, we use the following notation: Na_{743} and Li_{803} for the D-free fullerides and Li_{623_D}, Na_{523_D}, Na_{623_D} for the deuterated materials (see Table 1). The as-mixed composition of LiD and C_{60} is referred to as Li_{mix}. Solids and solvents were handled in a MBraun glove box under argon protective atmosphere.

All samples were analyzed by PND and SANS. PND data were collected at room temperature with the PUS diffractometer (λ=1.555 Å) at the JEEP II reactor (Kjeller, Norway).[47] During the measurements, powders were loaded into 6 mm vanadium container and sealed with indium wire. To extract information on symmetry of the formed crystalline phases and sizes of their unit cells, either Rietveld or Le Bail refinements were performed with the FullProf Suite program.[48] The diffraction profiles were modelled with a pseudo-Voigt peak shape function and the background was defined by interpolation between manually chosen points.

SANS experiments were also carried out at the JEEP II reactor. The q range employed in the experiments was 0.008–0. 25 $Å^{-1}$. The samples were filled in 1 mm Hellma quartz cuvettes, which were placed onto a copper-base in the sample chamber. The space between the sample and the detector was evacuated to reduce air scattering. For all samples it was ensured that the transmission was sufficiently high (> 90%), to disregard multiple scattering. Standard reductions of the scattering data, including transmission corrections, were conducted by incorporating data collected from an empty cell, a beam without cell and blocked-beam background. The data were transformed to an absolute scale by calculating the normalized scattered intensity from direct beam measurements.

Synchrotron radiation powder X-ray diffraction (SR-PXD) was performed at the Swiss-Norwegian Beamlines (SNBL, BM01A and BM01B). The samples were contained in 0.5 mm boronglass capillaries that were rotated during data collection to improve powder averaging. Wavelengths of 0.50513 Å and 0.80607 Å were used and 2D-diffraction data were collected with

a Dexela-Perkin Elmer 2923 CMOS detector[49] and a Pilatus 2M detector[50]. The program Bubble[50] was used to integrate the 2D diffraction images into 1D diffraction patterns.

3. Results and Discussion

3.1 Powder Neutron Diffraction (PND)

Li- and Na-intercalated fullerides along with their deuterated forms were investigated by PND (Figure 1 and 2).

Table 1. Synthesis details and samples notation used for the studied Na- and Li-based fullerides.

system	sample name	synthesis details
Na_6C_{60}–D_y		
	Na_{743}	mixture of C_{60}:6NaD annealed at 743 K
	Na_{523_D}	Na_{743} annealed under 100 bar of D_2 at 523 K
	Na_{623_D}	Na_{743} annealed under 100 bar of D_2 at 623 K
Li_6C_{60}–D_y		
	Li_{mix}	untreated mixture of C_{60}:6LiD
	Li_{623_D}	Li_{mix} annealed: under vacuum at 773 K, and subsequently under 100 bar of D_2 at 623 K
	Li_{803}	Li_{623_D} desorbed at 803 K

Li-based fullerides

The PND pattern of Li_{mix} (Figure 1a) shows exclusively the C_{60} phase but the cubic LiD (*Fm*-3*m*, a = 4.07 Å) is also present in the sample, as demonstrated by the laboratory powder X-ray diffraction data (not shown here). The poor visibility of the lithium deuteride diffraction peaks is likely due to its low abundance in the sample (ca. 6 wt.%) and an increased intensity of diffuse scattering resulting from presence of an amorphous component(s) in the material. The Li_{mix} PND data were analyzed by Rietveld refinements against various C_{60} structure models.[23, 31] The best agreement was obtained for the disordered C_{60} phase (*Fm*-3*m*) with a = 14.170(4) Å, and thus in line with published results.[31, 51-52] After D-desorption at 803 K significant changes appear in this sample (Figure 1b). The PND data show broadening of Bragg peaks for formed phase(s) indicating poor sample crystallinity. Moreover, the significant increase of the

background intensity suggests a high contribution of amorphous component(s). The low signal/noise ratio of the obtained data hindered proper Rietveld refinements but allowed for Le Bail analysis. The results confirm formation of the *fcc* Li_xC_{60} phase, with a smaller unit cell parameter, a = 13.99(3) Å, than that of pristine C_{60}. The lattice contraction is a commonly observed behavior, resulting from the Columbic interaction between Li cations and C_{60} anions. It demonstrates intercalation of Li atoms into the fullerite structure and crystallization of the Li_xC_{60} phase. Similar shrinkage of the unit cell associated with the Li-incorporation into C_{60} has been reported for $Li_{12}C_{60}$[19-20, 23] and Li_6C_{60}.[15, 21, 26, 34] The refined lattice constant of the cubic Li_xC_{60} is comparable to values previously obtained for the same phase by PXD, a = 14.03[26] and 14.04(2)[34] Å, and slightly bigger than in reported PND study, a =13.815(6) Å.[21] However, a closer look at the diffraction profile of the D-free Li_{803}, suggests formation of another crystalline phase in addition to Li_xC_{60}. This is in line with earlier reports, which reveal that the Li_6C_{60} system tends to crystallize with a minor fraction of Li_4C_{60}.[21, 34, 36-37] Unfortunately, due to limited resolution of the present PND data, this cannot be confirmed unambiguously in the Li_{803} sample.

The PND pattern of the D-containing Li_{623_D} looks significantly different from that of Li_{803} and indicates deuterium-induced structural changes (Figure 1c). The main identified phase, most likely $Li_xC_{60}D_y$, constitutes 95(5) wt.% of the sample and crystallizes with a *bcc* atomic arrangement (*Im*-3), a = 11.797(4) Å. It is similar to compounds reported earlier for $Li_{12}C_{60}$-$H(D)_y$[19-20] and Li_6C_{60}-$H(D)_y$.[21, 26, 34] The *bcc* $Li_xC_{60}D_y$ crystal structure is unknown, and based on the good quality of the Li_{623_D} PND data, we made an attempt to perform Rietveld refinements on our diffraction pattern. The atomic configuration of the *bcc* M_6C_{60} (*Im-3*), M = Cs, K, Rb, was used as a starting model.[53] At the first stage of the analysis, the contribution of Li and/or D atoms to the structure was neglected and the refinement was done exclusively with C atoms fully occupying designated crystallographic sites (C_1 at *24g*, C_2 at *48h*$_1$, C_3 at *48h*$_2$). This approach gave a partial agreement between observed and calculated data. However, the results indicated a strong disorder in the C_{60} lattice, as values of the atomic displacement parameters (B_{iso}) were high. In the next step, Li atoms were added to the model and their occupancy at tetrahedral and/or octahedral sites were refined. A significantly worse data fit was observed for all tested configurations, except for a model, in which Li atoms partly occupied the *12e* site (ca. 8 %). Interestingly, the agreement between observed and calculated data further improved when the same position was shared simultaneously by both Li and D atoms, 8 vs. 92 %, respectively (final

fit in Figure 1c). Presence of lithium and/or deuterium in the C_{60} structure leads to relaxation of the fulleride lattice, what is reflected in lower B_{iso} values. However, still a significant disorder can be observed. The present refined unit cell parameter of the *bcc* $Li_xC_{60}D_y$, 11.797(4) Å, is slightly smaller than those reported earlier for the cubic $Li_6C_{60}D_y$ (11.85(2) Å[34] and 11.816(4) Å[21]). The observed D-induced *fcc* to *bcc* phase transition is attributed to loss of the spherical nature of the C_{60} molecule that occurs at a high level of the hydrogen/deuterium

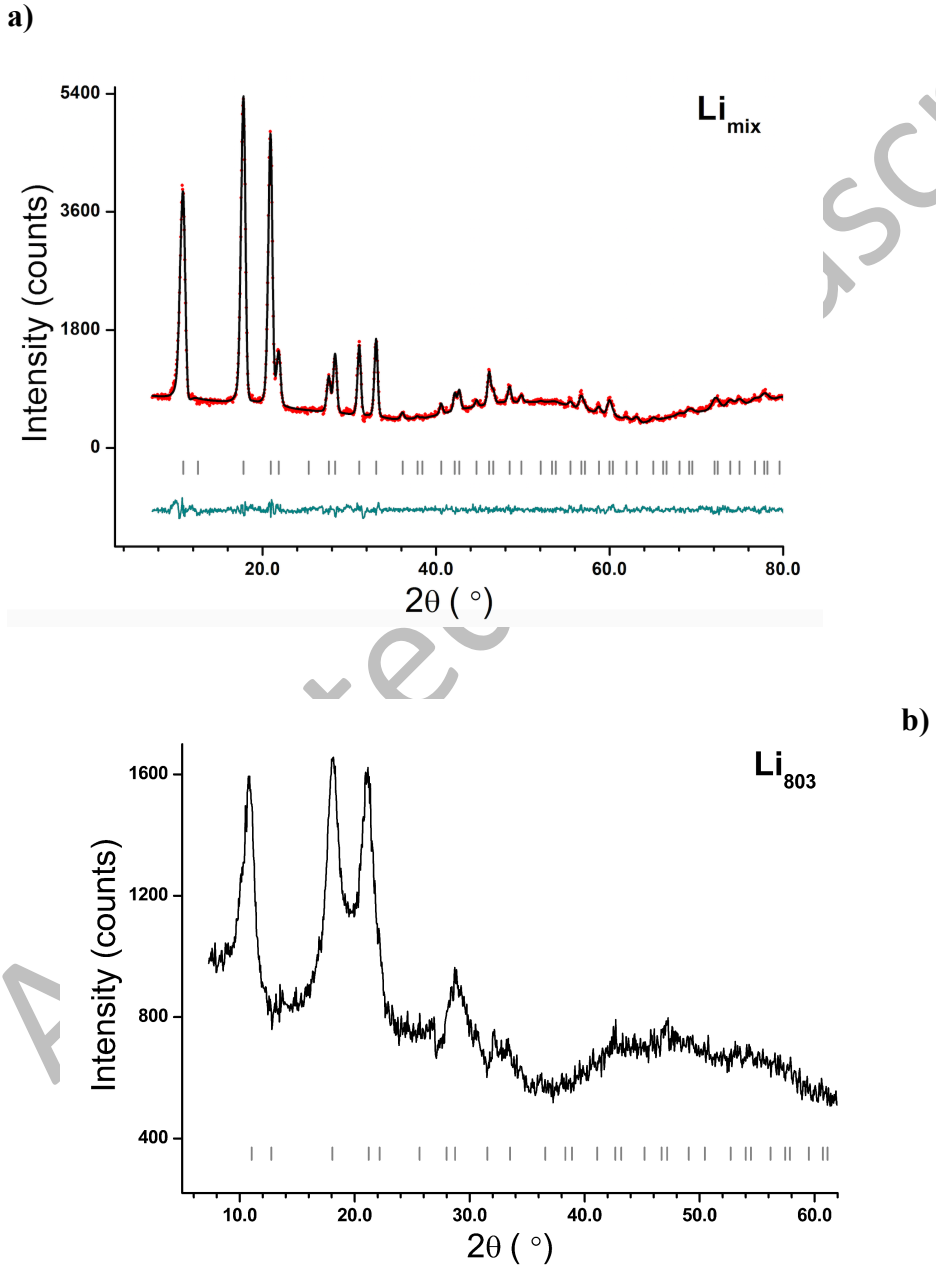

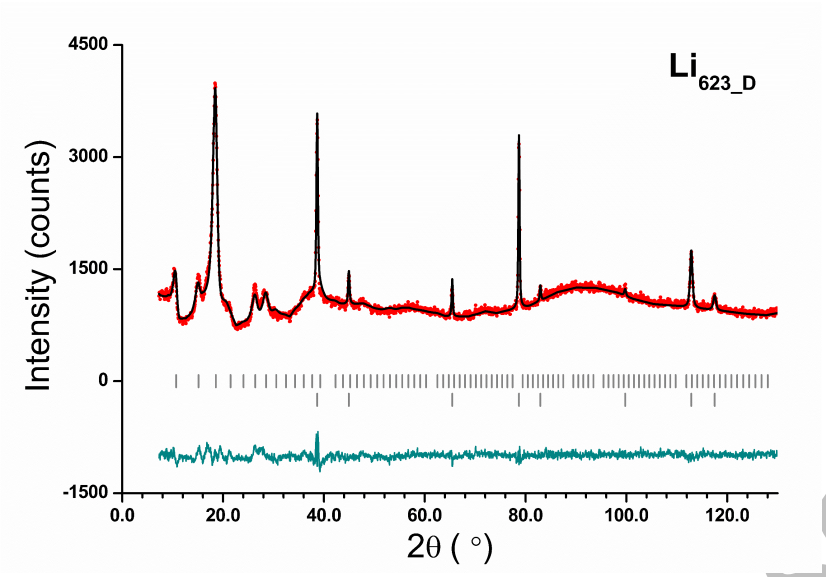

Figure 1. Graphical representation of Rietveld refinement fits for Li_{mix}, χ^2 = 2.97 (**a**) and Li_{623_D}, χ^2 = 1.60 (**c**); PND profile of Li_{803} (**b**); λ = 1.555 Å. Vertical bars represent position of Bragg reflections for identified phase: (**a**) C_{60}, (**b**) *fcc* Li_xC_{60} and (**c**) from top: *bcc* $Li_xC_{60}D_y$, LiD.

concentration in the system. Furthermore, in Li_{623_D}, the deuteration of Li_xC_{60} leads to a partial deintercalation of Li atoms from the fulleride and formation of LiD (5(1) wt.%), whose Bragg reflections reappear in the PND data (Figure 1c). This agrees well with previous studies reported for the Li_xC_{60}-$H(D)_y$ systems.[10, 19-21, 23, 25-26, 34, 44]

Na-based fullerides

One of the objectives of this work was to investigate crystal structures of Na-intercalated fullerides based on collected PND data. Unfortunately, the poor crystallinity of formed phases, significant abundance of amorphous component(s) in the materials and a multiphase nature of synthesized powders made Rietveld refinements impossible and hindered phase analysis for all Na-containing samples. For this reason, two years after preparation, all powders were re-investigated by SR-PXD, which provided higher resolution with superior statistics compared to PND and was thus expected to help in identification of crystalline compounds. The collected SR-PXD data allowed to discern Bragg peaks of formed phases but also demonstrated partial material decomposition /amorphisation (supporting information). Although, our phase analysis

provides fairly consistent results for both diffraction experiments, one cannot unambiguously confirm that phases present in the aged powders correspond exactly to the same sample compositions as found by PND. Nevertheless, the compounds identified by SR-PXD were used as a reference point for the phase analysis of the PND patterns.

The PND data collected for the Na_{743} sample are more complex than previously reported for the Na_xC_{60} systems and suggest the presence of multiple crystalline phases. This is surprising as literature data show that Na-incorporating fullerides, synthesized with the vapor phase method, crystallize mainly or exclusively as a single *fcc* fulleride.[15, 41] In Na_{743} coexistence of three crystalline compounds with different symmetries can be confirmed: *bcm*, *hcp* and *fcc*. The latter is most commonly observed in the D-free Na_xC_{60}.[15, 17, 20, 22, 25, 30, 32-33, 41] However, the formation of a hexagonal phase has been shown in the Na_xC_{60}-H(D) system, with $x \geq 4$.[24-25] A phase with monoclinic symmetry is typically present in Na_4C_{60}, which at RT crystallizes as a 2D polymeric phase.[33, 42-43] The lack of a structure model for the hexagonal phase as well as limited resolution of the PND made the quantitative phase analysis by Rietveld refinements impossible. However, the obtained results clearly show that the annealed mixture of C_{60} and NaD (1:6 molar

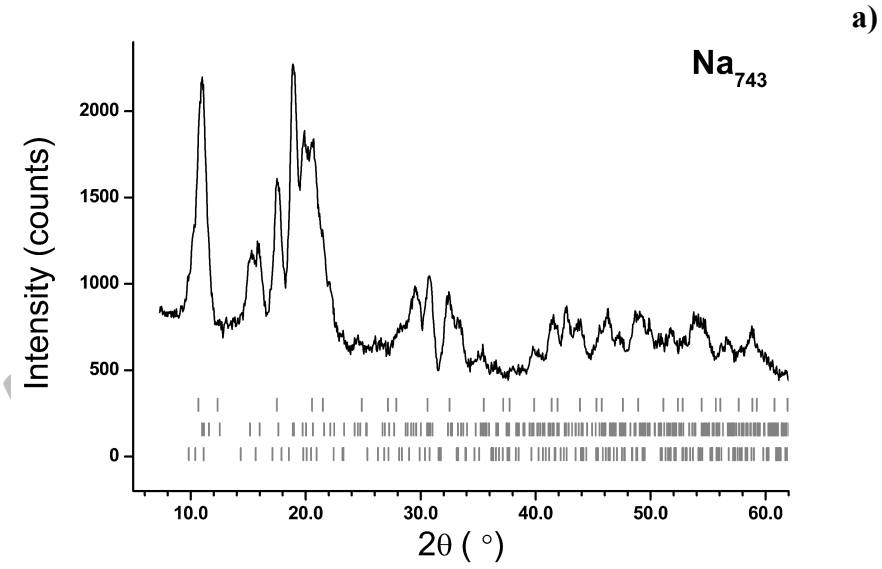

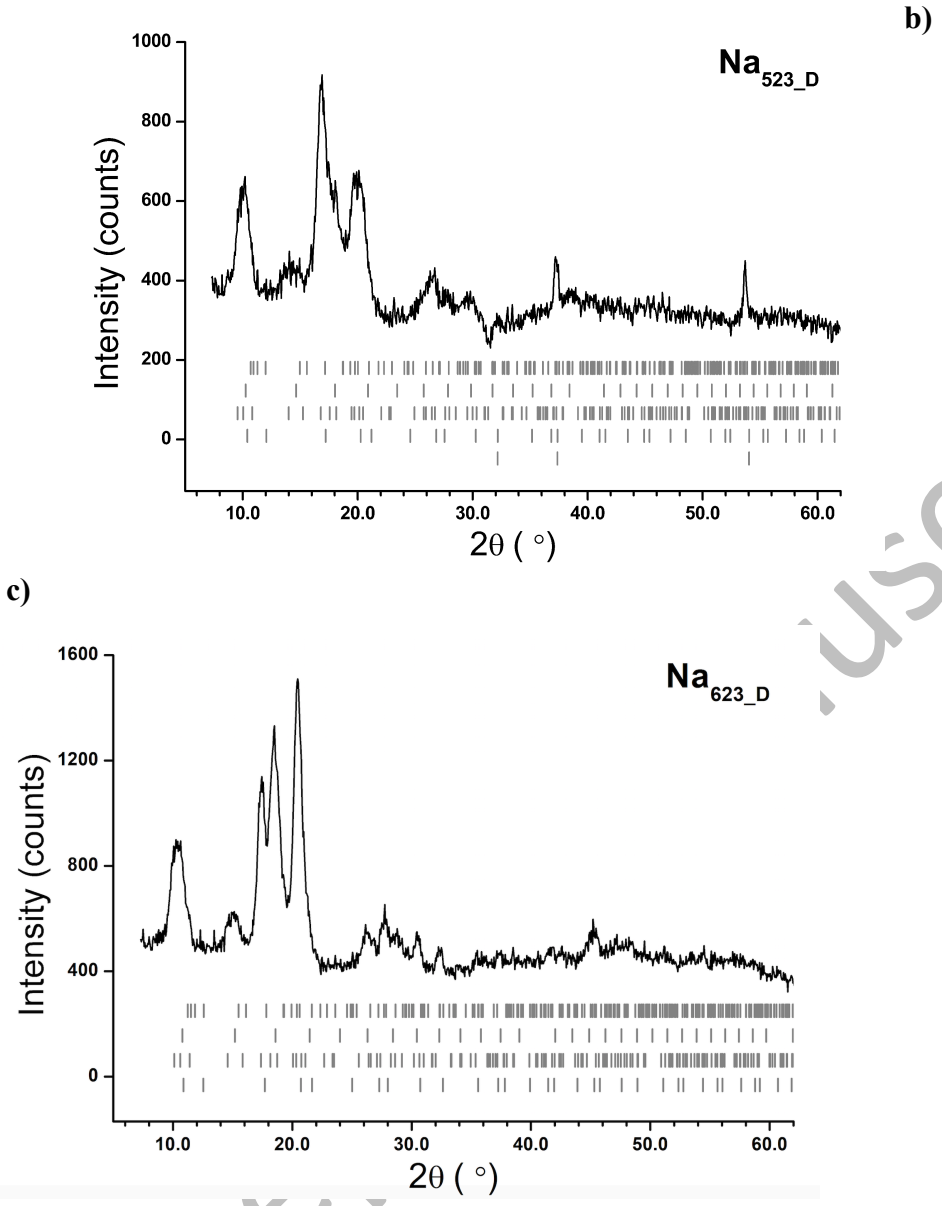

Figure 2. PND profiles of Na_{743} (**a**), Na_{523_D} (**b**) and Na_{623_D} (**c**); λ = 1.555 Å. Vertical bars represent position of Bragg reflections for identified phase, from top to bottom: (**a**) *fcc* Na_xC_{60}, *bcm* Na_xC_{60} and *hcp* Na_xC_{60}; (**b**) *bcm* Na_xC_{60}, *bcc* $Na_xC_{60}D_y$, *hcp* Na_xC_{60}, *fcc* $Na_xC_{60}D_y$ and NaD; (**c**) *bcm* Na_xC_{60}, *bcc* $Na_xC_{60}D_y$, *hcp* Na_xC_{60}, *fcc* $Na_xC_{60}D_y$.

ratio) forms a multiphase sample with various crystalline Na_xC_{60} structures rather than the phase-pure cubic Na_6C_{60} fulleride, as previously reported.[15, 17, 22, 30] On the other hand, similar to earlier

studies, the diffraction data of Na_{743} do not show presence of unreacted NaD and/or metallic Na, and thus suggesting a complete intercalation of Na into the fullerene structure.[20, 25, 27]

The deuterium-containing samples (Na_{523_D} and Na_{623_D}) reveal differences, when compared to the D-free powder. The phase analysis again suggests the presence of multiple Na_xC_{60} and/or $Na_xC_{60}D_y$ crystalline compounds. In addition to the *bcm*, *hcp* and *fcc* phases, also present in Na_{743}, NaD and a new crystalline structure with a *bcc* atomic arrangement are observed. The H(D)-induced crystallization of *bcc* $Na_xC_{60}H(D)_y$ has already been observed in the Na-intercalated fullerides at temperatures above 523 K and it was associated with the reversible *fcc–bcc* phase transition.[20, 25] For the Na_6C_{60}-H system, formation of the hydrogenated *bcc* phase was also reported but above 593 K and under 100 bar of H_2.[15, 17] In Na_{523_D}, deuteration of the fulleride(s) involves formation of NaD, which takes place at the expense of the Na atoms "leaking" from the intercalated Na_yC_{60} structures. This observation is in agreement with previous reports for the hydrogenated/deuterated Na_xC_{60}-H(D) systems.[17, 19-21, 25-26, 34]

The PND data of Na_{623_D} reveal further changes taking place in the material upon its deuteration at higher temperatures. The phase analysis confirms presence of structures with the same symmetries as in Na_{523_D}, except for NaD. This is similar to earlier observed processes occurring during hydrogenation (deuteration) of Na_xC_{60},[20, 25] where disappearance of NaD Bragg reflections was associated with a reversible intercalation of Na atoms into the fulleride(s).

3.2 Small Angle Neutron Scattering (SANS)

Li-based fullerides

Results from SANS experiments on the Li-based fullerides are presented in Figure 3. It can be seen that the Li-based fulleride samples scatter very well, covering more than 4 decades in intensity. The patterns show the typical behavior of a fractal-like system, with a constant log-log slope over nearly the entire measured q-range, as illustrated in the inset. Li_{623_D} containing deuterium (red) and the desorbed Li_{803} (blue) reveal a near similar scattering behavior (apart from at the highest q, as discussed below). Thus, the nanostructures of these two samples are quite similar. Sample Li_{mix} (green, as prepared), however, shows a different profile, with about a factor of two lower intensity in the low-q range than the others. This indicates that the Li_{mix} sample undergoes some nano-structural changes upon treatment.

The intensity level in the high-q limit is a measure of the amount of incoherent scattering from the sample. Although deuterium has an incoherent signal significantly smaller than hydrogen (ca. 1/10), its presence will contribute to the incoherent scattering. It is therefore reasonable that Li_{803} presents the lowest intensity at high q, since it does not contain deuterium. Li_{mix} and Li_{623_D}, which both contain deuterium, show higher intensities in that range, as expected. Based on the values observed in the high-q limit, there is a first indication that the amount of deuterium is somewhat less in Li_{623_D} than in Li_{mix}. However, one should note that the asymptotic levels of the curves have not been reached yet, and the differences in curve shapes could also be due to a slight restructuring at the smallest scales (around 1 nm) for Li_{623_D} compared to the as-mixed sample.

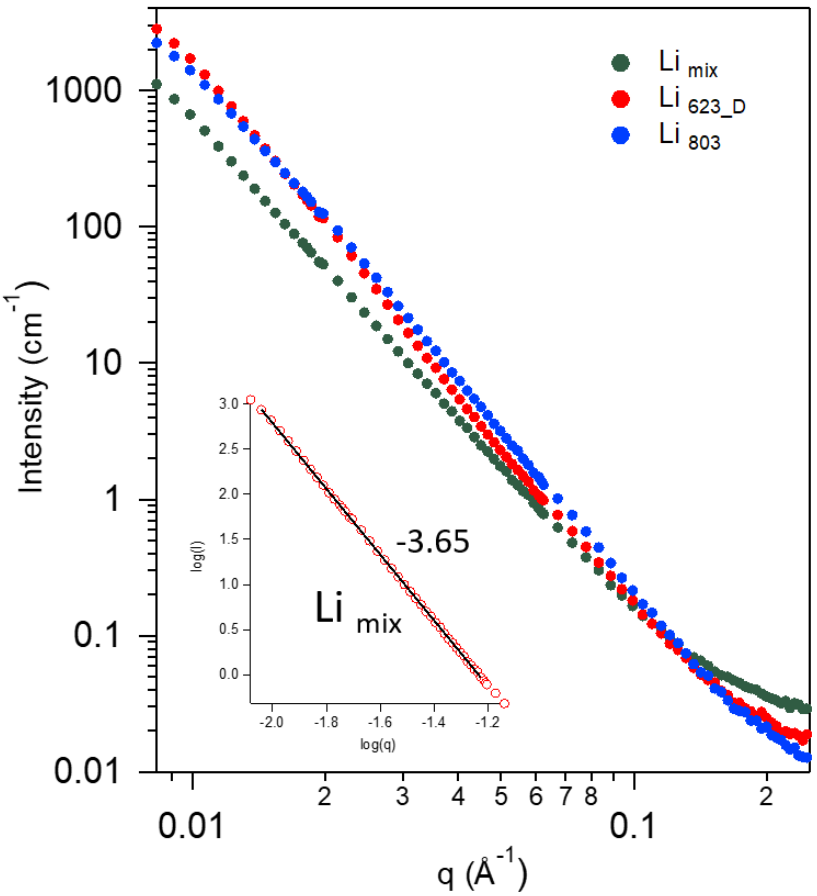

Figure 3. SANS on Li_{mix}, Li_{623_D}, and Li_{803}. The inset shows the constant log-slog slope over a large q-range, here for sample Li_{mix} with a slope of -3.65.

We employed the unified power-Rg model (Beaucage model) to analyze the SANS data from this system. This is a shape-independent model that has been shown to give a good representation of many systems that consist of individual particles with a certain polydispersity that can cluster together in structures with varying overall characteristic sizes Rg.[54-55] As can be seen from equation (1) below, this basic version of this function (1-level) is the combination of a Guinier term describing the intensity in the low-q region with Rg being the average size of the scattering objects (G gives the overall scaling of the intensity for this term), and a power-law term describing the scattering at mid/high-q (B gives the overall scaling of the intensity for this term).

$$I(\mathrm{q}) = G \exp(-q^2 Rg^2/3) + B \{[\ \mathrm{erf}(qRg/\sqrt{6})\ ]^3/q\}^{\alpha} + bgd \qquad (1)$$

Here α is the power law exponent. The term *bgd* is a background, and "erf" is the standard error function.

Figure 4 shows the whole pattern fitting for the various Li-composites. The bottom right in Figure 4 is an image of the three samples, where the as-prepared sample had initially a black color. During the absorption step the color changed from black to gray/brown (cuvette in the middle of the inset picture), and finally, after desorption it turned black again.

The log-log slope in the low-q region is measure of the surface properties of the particles in the sample. In all cases the slope (α) is found to be well above 3 in absolute value, characteristic of a surface fractal system. A slope of -4 represents a fully smooth surface, whereas values between 3 and 4 indicates a certain surface roughness. The surface fractal dimension is given by $Ds = 6–\alpha$, so that a completely smooth surface would give a Ds equal to 2.0.

The extracted power law slope for the three samples is as follows: Li_{mix} = - 3.63, Li_{623_D} = - 3.98, and Li_{803} = - 3.95. All these values are representative of surface fractals. However, the as-prepared sample (Li_{mix}) shows a rougher surface than the two others, with a surface fractal dimension $D_s = 6–\alpha = 2.37$, where the fully smooth surface would give a D_s equal to 2.0. Li_{623_D} is found to have the highest slope, corresponding well with visual inspection of Figure 5. In this case, the fractal dimension is 2.02, i.e. very close to a fully smooth surface.

The model fitting for the Li_{mix} sample results in a "particle" size of R_g = 28 nm. For sample Li_{623_D}, a value of R_g = 22 nm is obtained, whereas the desorbed sample, Li_{803}, presents a value of R_g = 27 nm. When comparing these three samples, we notice reduction in characteristic size (R_g) for Li_{623_D} compared to Li_{mix}. For Li_{803}, the characteristic size returns close to the value for Li_{mix}. The Rg-values extracted for the Li-fullerides must be interpreted with caution due to

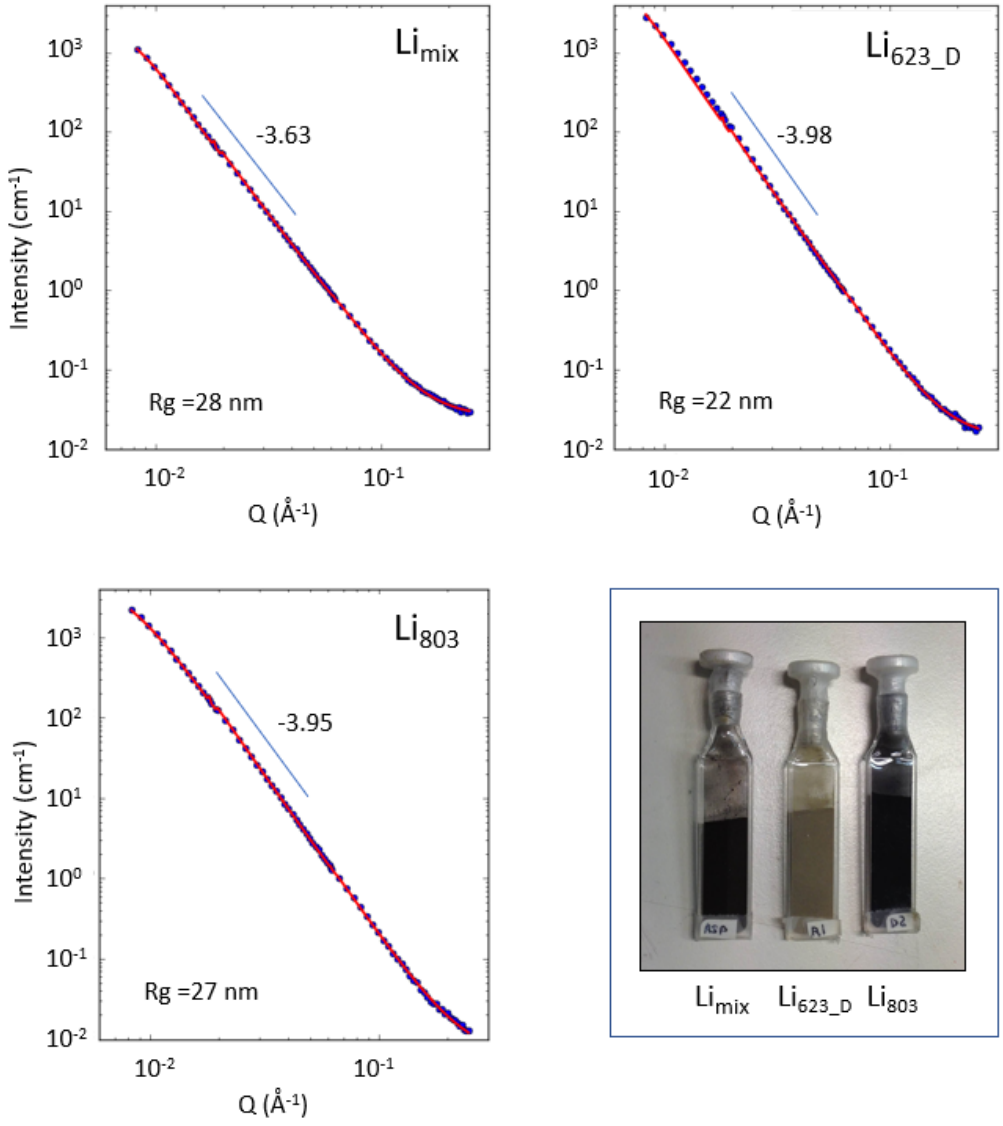

Figure 4. SANS data from Li-based composites with 1-level Beaucage model fitting. The power law slopes are indicated with a line together with the corresponding exponent.

the absence of a fully developed low-q plateau. However, the reduction in characteristic size when the sample is deuterated (Li_{623_D}), may well be an indication of fracture/disintegration of small-sized crystallites in the sample. Based on this interpretation, a partial return to a larger crystallite sizes likely occurs when the sample is desorbed (Li_{803}).

The SANS data correlates well with the PND results described earlier in terms of a significant difference between the as-prepared and D-absorbed/-desorbed samples. The PND data for Li_{623_D} indicate formation of phases connected with the inclusion of deuterium, and the corresponding SANS pattern shows an increase in the low-q slope, and a slight reduction in the

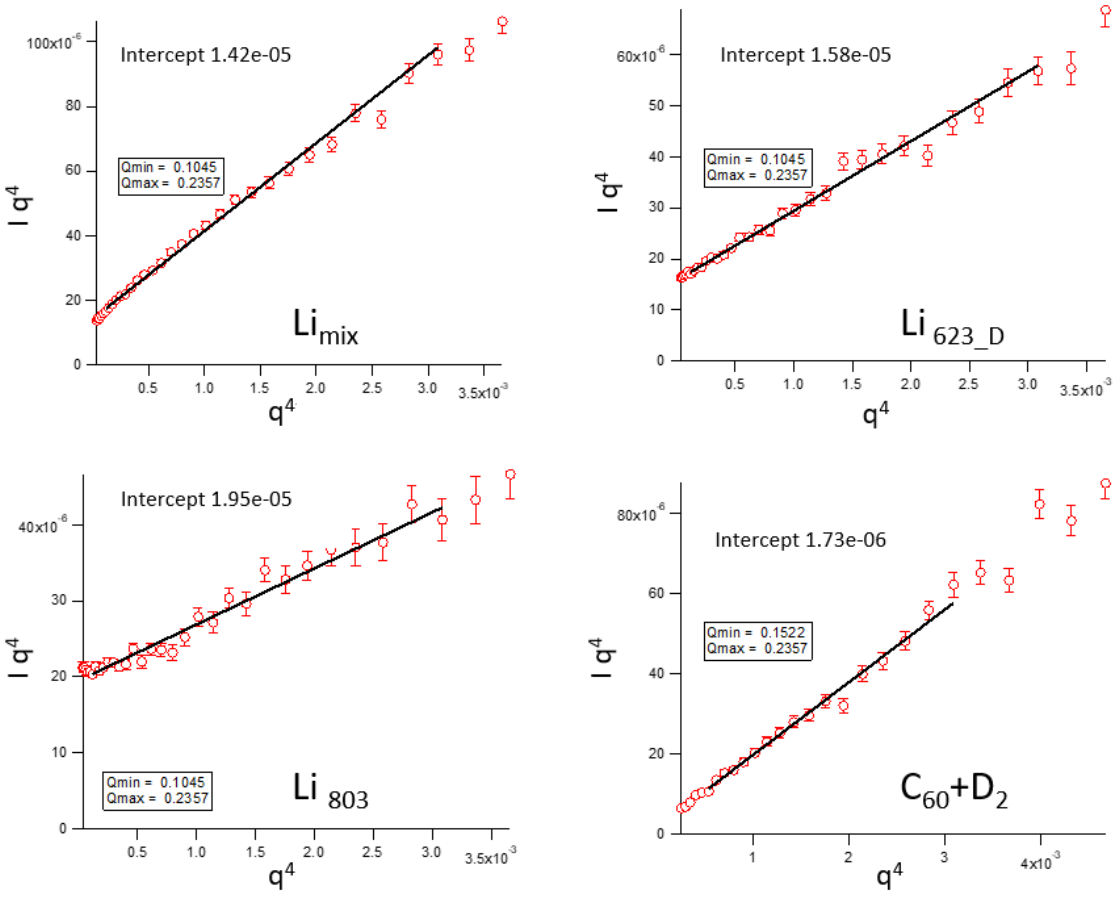

Figure 5. SANS data from Li-based composites plotted vs q^4 for extraction of specific surface via the y-axis intercept.

characteristic size. For the D-desorbed sample of Li_{803}, the PND data show disappearance of the LiD Bragg peaks, and the SANS pattern reveal a small, but clearly identified, slope reduction compared to Li_{623_D}. This is equivalent to an increased surface roughness (Ds = 6-3.95 = 2.05). During desorption of deuterium from the previously annealed samples, the incorporation of Li into the fullerene structure is accompanied by the effect of making the crystallite surface more rough or irregular. This change in surface morphology is possibly due to an increased local strain near the crystallite surface.

Specific surface

In the high-q limit, the SANS intensity is proportional of the surface per volume unit S_V:[56]

$$d\Sigma/d\Omega_{\ q->\infty} = (2\pi|\Delta\rho|^2\ S_V)/q^4 + bgd \qquad (2)$$

Here $\Delta\rho$ is the difference in scattering length density (SLD) between the material and the surrounding matrix. In the present case the surroundings are voids. The term *bgd* is the incoherent background, which depends on the specific elements present in the sample (and the concentration). Thus, by plotting q^4 times the scattered intensity ($d\Sigma/d\Omega$) vs. q^4 one should obtain a regression line ($y = ax+b$) by which S_V can be found from the intercept with the y-axis (and the background from the slope of the line). The intercept b equals $2\pi|\Delta\rho|^2\ S_V$, thus the specific surface is given by $S_V = b\ /\ (2\pi|\Delta\rho|^2)$. S_V has dimension $cm^2/cm^3 = cm^{-1}$, and can be converted to specific surface S_m (cm^2/g) by dividing by the specific weight ρ_m (g/cm^3). Such an analysis was done for a set of samples, as shown in Figure 5. Based on these results, we could obtain nominal values for the specific surface, as shown in Table 2. This analysis was done for the Li-based fullerides only, since they showed the best statistical quality. These results indicate an increase in the internal surface area for the deuterated sample (Li_{623_D}) compared to the as-prepared sample (Li_{mix}), and a further increase for the D-desorbed powder (Li_{803}). The scattering length density is not known a priori. However, we can estimate the SLD of the sample but by utilizing an approximate value of the specific gravity Li_6C_{60} (1.8 g/cm^3, not taking into account any D present). This results in a specific surface of Li_{mix} of 7.5e+04 cm^{-1} (or 4.2e+04 when measured in cm^2/g). The changes observed could be due to fracturing of the crystallites in the sample and increase in the specific surface area after absorption of deuterium. If so, it seems that the surface

structure is not recovered, but rather progresses further when the hydrogen is desorbed (803 K). It should be noted that the fractal exponents commented on earlier (cf. Figure 4) indicate that the surface roughness is in any case relatively low (exponent close to -4) after deuterium loading / desorption. Thus, although a change in roughness can in principle also contribute to the specific surface, the main contribution to the changes in surface area shown above are likely to be crystallite fracture and a corresponding modification in the number of crystallites per volume unit.

Table 2. Estimated specific surfaces for the Li-based fullerides based on SANS data. *: SLD-value uncertain since the specific volume is not known exactly.

sample	intercept [cm^{-1} $Å^{-4}$]	SLD [$Å^{-2}$]	specific surface S_V [cm^{-1}]	specific surface [cm^2/g]
Li_{mix}	1.4273e-05	5.5 e-06	7.5 e+04	4.2 e+04
Li_{623_D}	1.5825e-05	5.5 e-06*	8.3 e+04	4.6 e+04
Li_{803}	1.9483e-05	5.5 e-06*	1.02 e+05	5.6 e+04

Na-based fullerides

The SANS data for the Na-based fullerides are presented in Figure 6. The samples show an overall similar type of behavior, with strong scattering towards low q-values, and an intensity covering more than 4 decades. The difference in absolute intensities observed in the low-q range may be partly attributed to a slight variation in effective packing density for the different powder samples inside the sample cuvette. However, some other differences can be seen between the samples, for example in the mid/high q range. This range corresponds to small length scales, on the order of 1-10 nm. There are also weak signs of slightly reduced scattering slope at the lowermost q-values, corresponding to larger scales, of approximately 30 nm. Furthermore, as commented for the Li-based system, there should be a lower asymptotic level at high q for deuterium-free samples. As expected, this is also what we observe for the Na_{743} sample.

Figure 7 shows the different Na-based samples as well as the $C_{60} + D_2$ sample as individual plots, together with their corresponding fitted model curves. We see that Na_{623_D} has slightly lower power law slope, thus a rougher internal surface than the other two samples. For the pure C_{60} we find a slope closer to -4, but in fact with an absolute value slightly above 4. This

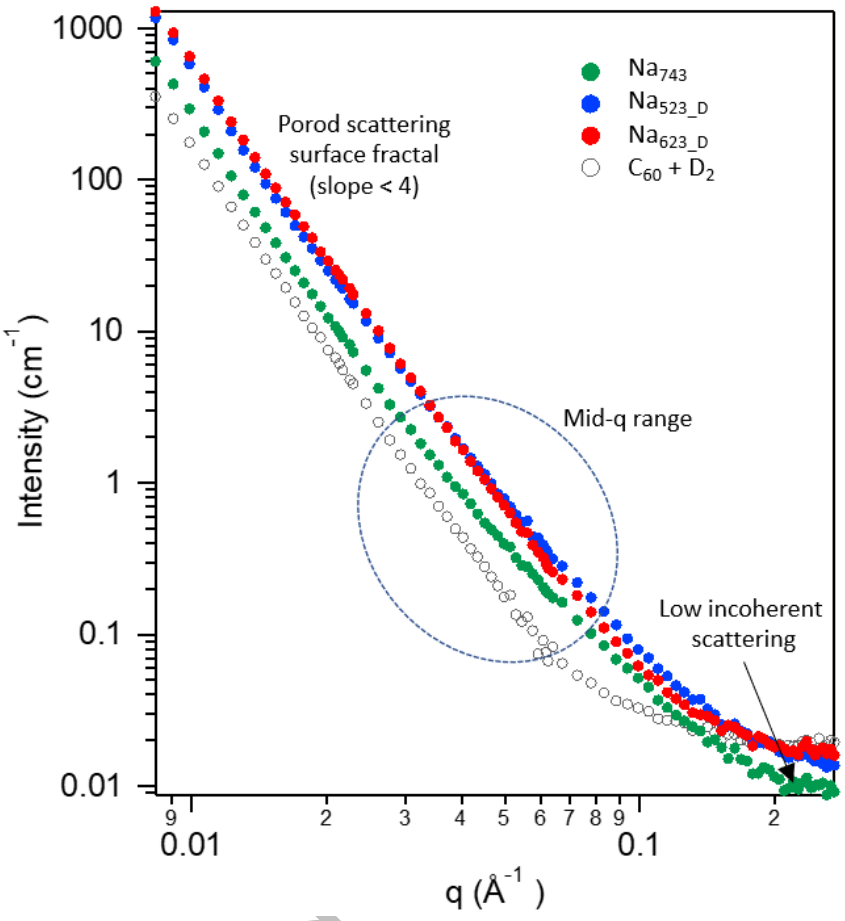

Figure 6. SANS data from the Na-based fullerides Na_{743}, Na_{523_D} and Na_{623_D}, as well as the Na-free sample $C_{60} + D_2$.

indicates a smooth surface structure, but with an interface region that is slightly diffuse, e.g. with a non-abrupt transition between the particle and surrounding voids in terms of scattering length density.

We note that none of the samples presents any saturation of the intensity at low q-values. However, there is a slight reduction of the slope in the low-q limit for some of the Na-based samples (Na_{743} and Na_{523_D}), indicating that we approach a characteristic size of the structures (such an effect cannot be seen for Na_{623_D} or the pure $C_{60} + D_2$ sample). The Beaucage model provides the Rg-value of 29 nm for both Na_{743} and Na_{523_D}. Since there is no developed plateau in the low-q region, the fitted Rg-values are apparent sizes, representing structures within the size window that can be probed with SANS (up to ca. 50 nm). Larger structures, e.g.

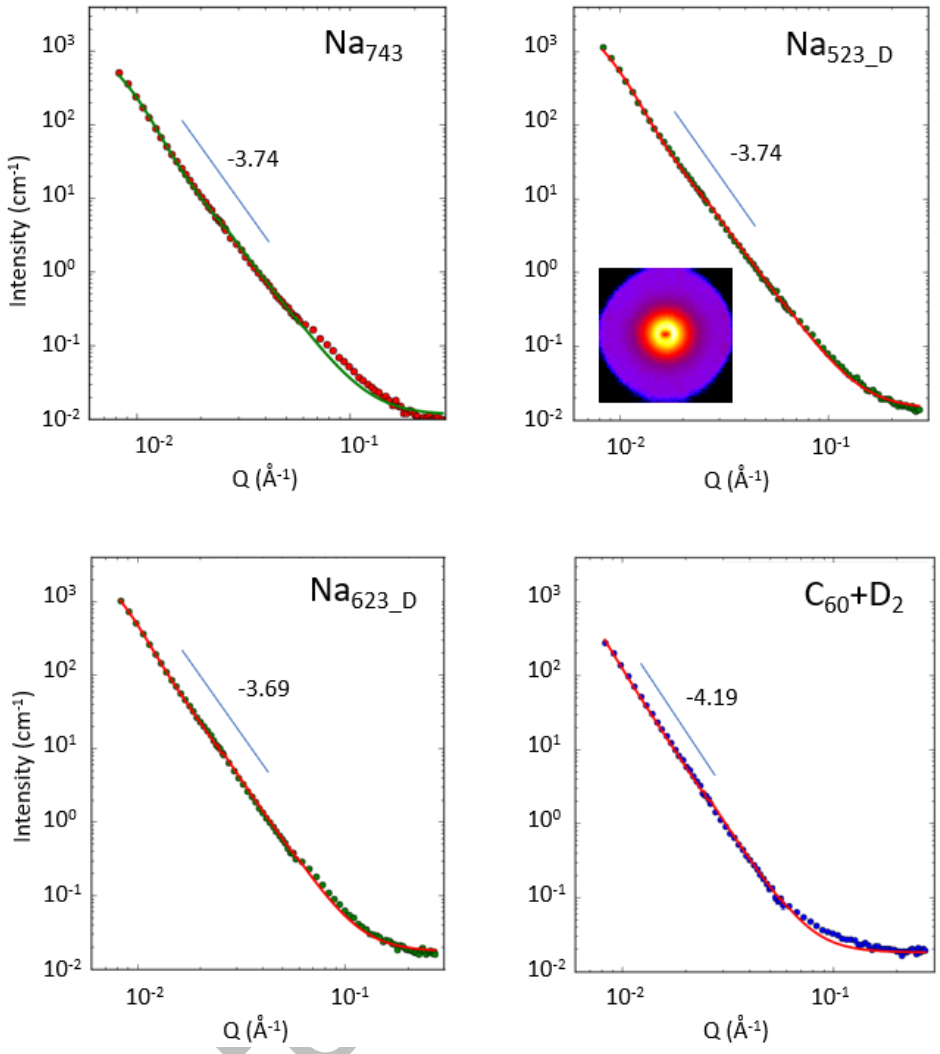

Figure 7. SANS data from Na-based fullerides with 1-level Beaucage model fitting. The power law slopes are indicated with a straight line together with the corresponding exponent. The inset in the upper right figure is an example of the collected 2D SANS image (here for Na_{523_D})

crystallites, are surely also present in the sample. The extracted Rg-values must therefore be interpreted with caution, but may indicate tendencies of internal changes under different loading conditions.

The SANS data do not show any significant structural changes for Na_{523_D} as compared to Na_{743}. Both, the fractal dimension and the apparent characteristic size (R_g) are found to be similar for these two samples. However, for the sample annealed at the highest temperature (Na_{623_D}), a slight reduction in the low-q slope (α) is identified and corresponds to an increase in

the surface roughness (Ds = 6 - |α| = 2.3). This is very similar to our observations in the Li-fullerides. When comparing with the PND data, annealing at 743 K is found to be correlated with the disappearance of the crystalline NaD peak. It is therefore possible that the morphological changes seen from SANS are linked to this effect, i.e. to the intercalation of Na into the fulleride, with a corresponding increased surface roughness.

4. Conclusion

Results of SANS data analysis for Li- and Na-based fullerides indicate certain nano-structural changes occurring with the incorporation of Li and Na into the material. The pure C_{60} + D_2 is found to have a near smooth crystallite surface structure but with indications of a slight variation in mass density close to the crystallite surface. However, the mixed fullerene and Li-/Na-based materials present more rough interfaces, with surface fractal dimensions in the range 2-2.4. The PND data analysis shows disappearance of the crystalline LiD/NaD Bragg peaks after deuterium desorption. From SANS data, this process, associated with incorporation of Li/Na into the fullerene structure, could be linked to an increase in the crystallite surface roughness. Furthermore, the specific internal surface of the material is found to increase after deuterium absorption and subsequent desorption, and likely to result in a moderate fracturing of crystallites. Finally, SANS measurements appear as an instructive way to follow directly the incorporation and/or release of deuterium via the level of incoherent scattering in the high-q limit of the SANS diagram.

Acknowledgements

The authors acknowledge the skillful assistance from the staff of the Swiss-Norwegian Beamlines (SNBL), at the European Synchrotron Radiation Facility (ESRF), Grenoble, France. Work at SRNL was supported by the U.S. Department of Energy, Office of Science, Basic Energy Sciences, Materials Sciences and Engineering Division.

Supporting Information

The Supporting Information is available free of charge on the ACS Publications website http://pubs.acs.org:

Graphical representations of Le Bail refinements on SR-PXD data for Na- intercalated samples.

References:

1. Weaver, J. H.; Poirier, D. M., Solid State Properties of Fullerenes and Fullerene-Based Materials. *Solid State Phys* **1994**, *48*, 1-108.
2. Lieber, C. M.; Zhang, Z., Physical Properties of Metal-Doped Fullerene Superconductors. *Solid State Phys* **1994**, *48*, 349-384.
3. Tanigaki, K.; Prassides, K., Conducting and Superconducting Properties of Alkali-Metal C_{60} Fullerides. *J Mater Chem* **1995**, *5*, 1515-1527.
4. Kim, M.; Nomura, Y.; Ferrero, M.; Seth, P.; Parcollet, O.; Georges, A., Enhancing Superconductivity in A_3C_{60} Fullerides. *Phys Rev B* **2016**, *94*, 155152.
5. Takabayashi, Y.; Prassides, K., The Renaissance of Fullerene Superconductivity. *Struct Bond* **2016**, *172*, 119-138.
6. Ganin, A. Y.; Takabayashi, Y.; Jelič, P.; Arčon, D.; Potočnik, A.; Baker, P. J.; Ohishi, Y.; McDonald, M. T.; Tzirakis, M. D.; McLennan, A., et al., Polymorphism Control of Superconductivity and Magnetism in Cs_3C_{60} Close to the Mott Transition. *Nature* **2010**, *466*, 221-225.
7. Pontiroli, D.; Riccò, M.; Shiroka, T.; Belli, M.; Ruani, G.; Palles, D.; Margadonna, S., New Polymeric Phase in Low-Doped Lithium Intercalated Fullerides. *Fuller Nanotub Car N* **2006**, *14*, 391-400.
8. Riccò, M.; Shiroka, T.; Belli, M.; Pontiroli, D.; Pagliari, M.; Ruani, G.; Palles, D.; Margadonna, S.; Tomaselli, M., Unusual Polymerization in the Li_4C_{60} Fulleride. *Phys Rev B* **2005**, *72*, 155437.
9. Wagberg, T.; Stenmark, P.; Sundqvist, B., Structural Aspects of Two-Dimensional Polymers: Li_4C_{60}, Na_4C_{60} and Tetragonal C_{60}. Raman Spectroscopy and X-Ray Diffraction. *J Phys Chem Solids* **2004**, *65*, 317-320.
10. Riccò, M.; Belli, M.; Mazzani, M.; Pontiroli, D.; Quintavalle, D.; Jánossy, A.; Csányi, G., Superionic Conductivity in the Li_4C_{60} Fulleride Polymer. *Phys Rev Lett* **2009**, *102*, 145901.
11. Pontiroli, D.; Aramini, M.; Gaboardi, M.; Mazzani, M.; Gorreri, A.; Riccò, M.; Margiolaki, I.; Sheptyakov, D., Ionic Conductivity in the Mg Intercalated Fullerene Polymer Mg_2C_{60}. *Carbon* **2013**, *51*, 143-147.
12. Sundqvist, B.; Yao, M. G.; Wagberg, T., Electrical Transport Properties of A_4C_{60} (A=Li, Na and Rb) under Pressure. *High Pressure Res* **2008**, *28*, 597-600.
13. Sundqvist, B.; Wagberg, T.; Yao, M. G., High Pressure Studies of Alkali Metal Doped Fullerides A_4C_{60}. *Diam Relat Mater* **2011**, *20*, 600-603.
14. Teprovich, J. A.; Knight, D. A.; Wellons, M. S.; Zidan, R., Catalytic Effect of Fullerene and Formation of Nanocomposites with Complex Hydrides: $NaAlH_4$ and $LiAlH_4$. *J Alloy Compd* **2011**, *509*, 562-566.
15. Teprovich, J. A.; Knight, D. A.; Peters, B.; Zidan, R., Comparative Study of Reversible Hydrogen Storage in Alkali-Doped Fulleranes. *J Alloy Compd* **2013**, *580*, 364-367.
16. Paolone, A.; Palumbo, O.; Leardini, F.; Cantelli, R.; Knight, D. A.; Teprovich, J. A.; Zidan, R., A Spectroscopic Investigation of Hydrogenated Li Doped Fullerane. *J Alloy Compd* **2013**, *580*, S67-S69.
17. Knight, D. A.; Teprovich, J. A.; Summers, A.; Peters, B.; Ward, P. A.; Compton, R. N.; Zidan, R., Synthesis, Characterization and Reversible Hydrogen Sorption Study of Sodium-Doped Fullerene. *Nanotechnology* **2013**, *24*, 455601.
18. Ward, P. A.; Teprovich, J. A.; Peters, B.; Wheeler, J.; Compton, R. N.; Zidan, R., Reversible Hydrogen Storage in a $LiBH_4$-C_{60} Nanocomposite. *J Phys Chem C* **2013**, *117*, 22569-22575.
19. Mauron, P.; Gaboardi, M.; Remhof, A.; Bliersbach, A.; Sheptyakov, D.; Aramini, M.; Vlahopoulou, G.; Giglio, F.; Pontiroli, D.; Riccò, M., et al., Hydrogen Sorption in $Li_{12}C_{60}$. *J Phys Chem C* **2013**, *117*, 22598-22602.
20. Mauron, P.; Gaboardi, M.; Pontiroli, D.; Remhof, A.; Riccò, M.; Züttel, A., Hydrogen Desorption Kinetics in Metal Intercalated Fullerides. *J Phys Chem C* **2015**, *119*, 1714-1719.

21. Gaboardi, M.; Duyker, S.; Milanese, C.; Magnani, G.; Peterson, V. K.; Pontiroli, D.; Sharma, N.; Riccò, M., In Situ Neutron Powder Diffraction of Li_6C_{60} for Hydrogen Storage. *J Phys Chem C* **2015**, *119*, 19715-19721.
22. Gaboardi, M.; Milanese, C.; Magnani, G.; Girella, A.; Pontiroli, D.; Cofrancesco, P.; Marini, A.; Riccò, M., Optimal Hydrogen Storage in Sodium Substituted Lithium Fullerides. *Phys Chem Chem Phys* **2017**, *19*, 21980-21986.
23. Giglio, F.; Pontiroli, D.; Gaboardi, M.; Aramini, M.; Cavallari, C.; Brunelli, M.; Galinetto, P.; Milanese, C.; Riccò, M., $Li_{12}C_{60}$: A Lithium Clusters Intercalated Fulleride. *Chem Phys Lett* **2014**, *609*, 155-160.
24. Kobayashi, M.; Kimata, N.; Heguri, S., X-ray Diffraction and Magnetic Susceptibility of Sodium Fullerides Na_xC_{60}. *J Phys Chem Solids* **2010**, *71*, 689-691.
25. Mauron, P.; Remhof, A.; Bliersbach, A.; Riccò, M., Reversible Hydrogen Absorption in Sodium Intercalated Fullerenes. *Int J Hydrogen Energ* **2012**, *37*, 14307-14314.
26. Teprovich, J. A.; Wellons, M. S.; Lascola, R.; Hwang, S. J.; Ward, P. A.; Compton, R. N.; Zidan, R., Synthesis and Characterization of a Lithium-Doped Fullerane (Li_x-C_{60}-H_y) for Reversible Hydrogen Storage. *Nano Lett* **2012**, *12*, 582-589.
27. Gaboardi, M.; Sarzi Amadè, N.; Riccò, M.; Milanese, C.; Girella, A.; Gioventù, M.; Fernandez-Alonso, F., Synthesis and Characterization of Mixed Sodium and Lithium Fullerides for Hydrogen Storage. *Int J Hydrogen Energ* **2018**, https://doi.org/10.1016/j.ijhydene.2018.03.210.
28. Amade, N. S.; Pontiroli, D.; Maidich, L.; Riccò, M.; Gaboardi, M.; Magnani, G.; Carretta, P.; Sanna, S., Molecular and Ionic Dynamics in $Na_xLi_{6-x}C60$. *J Phys Chem C* **2017**, *121*, 6554-6560.
29. Aramini, M.; Milanese, C.; Pontiroli, D.; Gaboardi, M.; Girella, A.; Bertoni, G.; Riccò, M., Addition of Transition Metals to Lithium Intercalated Fullerides Enhances Hydrogen Storage Properties. *Int J Hydrogen Energ* **2014**, *39*, 2124-2131.
30. Rosseinsky, M. J.; Murphy, D. W.; Fleming, R. M.; Tycko, R.; Ramirez, A. P.; Siegrist, T.; Dabbagh, G.; Barrett, S. E., Structural and Electronic Properties of Sodium-Intercalated C_{60}. *Nature* **1992**, *356*, 416-418.
31. Yildirim, T.; Zhou, O.; Fischer, J. E.; Bykovetz, N.; Strongin, R. A.; Cichy, M. A.; Smith, A. B.; Lin, C. L.; Jelinek, R., Intercalation of Sodium Heteroclusters into the C_{60} Lattice. *Nature* **1992**, *360*, 568-571.
32. Yildirim, T.; Fischer, J. E.; Harris, A. B.; Stephens, P. W.; Liu, D.; Brard, L.; Strongin, R. M.; Smith, A. B., Orientational Phase Transition in Na_xC_{60} (1<x<3). *Phys Rev Lett* **1993**, *71*, 1383-1386.
33. Kubozono, Y.; Takabayashi, Y.; Kambe, T.; Fujiki, S.; Kashino, S.; Emura, S., Structure and Physical Properties of Na_4C_{60} under Ambient and High Pressures. *Phys Rev B* **2001**, *63*, 045418.
34. Maidich, L.; Pontiroli, D.; Gaboardi, M.; Lenti, S.; Magnani, G.; Riva, G.; Carretta, P.; Milanese, C; Marini, A.; Riccò, M., et al., Investigation of Li and H Dynamics in Li_6C_{60} and $Li_6C_{60}H_y$. *Carbon* **2016**, *96*, 276-284.
35. Cristofolini, L.; Cicognani, G.; Dianoux, A. J.; Facci, P.; Fontana, M. P.; Riccò, M., Li Diffusion and Fullerene Dynamics in Lithium Fulleride $Li_{12}C_{60}$ from Inelastic Neutron Scattering Experiments. *Philos Mag B* **1999**, *79*, 2065-2071.
36. Margadonna, S.; Pontiroli, D.; Belli, M.; Shiroka, T.; Riccò, M.; Brunelli, M., Li_4C_{60}: A Polymeric Fulleride with a Two-Dimensional Architecture and Mixed Interfullerene Bonding Motifs. *J Am Chem Soc* **2004**, *126*, 15032-15033.
37. Riccò, M.; Belli, M.; Pontiroli, D.; Mazzani, M.; Shiroka, T.; Arčon, D.; Zorko, A.; Margadonna, S.; Ruani, G., Recovering Metallicity in A_4C_{60}: The Case of Monomeric Li_4C_{60}. *Phys Rev B* **2007**, *75*, 081401.
38. Arčon, D.; Zorko, A.; Mazzani, M.; Belli, M.; Pontiroli, D.; Riccò, M.; Margadonna, S., The Structural and Electronic Evolution of Li_4C_{60} Through the Polymer-Monomer Transformation. *New J Phys* **2008**, *10*, 033021.

39. Tomaselli, M.; Meier, B. H.; Riccò, M.; Shiroka, T.; Sartori, A., A Multiple-Quantum Nuclear Magnetic Resonance Study of Interstitial Li Clusters in Li_xC_{60}. *J Chem Phys* **2001**, *115*, 472-476.
40. Aramini, M.; Gaboardi, M.; Vlahopoulou, G.; Pontiroli, D.; Cavallari, C.; Milanese, C.; Riccò, M., Muon Spin Relaxation Reveals the Hydrogen Storage Mechanism in Light Alkali Metal Fullerides. *Carbon* **2014**, *67*, 92-97.
41. Kulbachinskii, V. A.; Bulychev, B. M.; Kytin, V. G.; Krechetov, A. V.; Tarasov, V. P.; Konstantinova, E. A.; Velikodnyi, Y. A.; Muravlev, Y. B.; Zoteev, A. V., Magnetic and Structural Anomalies of Na_nC_{60} (n=2, 3). *Cent Eur J Phys* **2010**, *8*, 101-112.
42. Oszlányi, G.; Baumgartner, G.; Faigel, G.; Forró, L., Na_4C_{60}: An Alkali Intercalated Two-Dimensional Polymer. *Phys Rev Lett* **1997**, *78*, 4438-4441.
43. Oszlányi, G.; Baumgartner, G.; Faigel, G.; Granasy, L.; Forró, L., Polymer-Monomer Phase Transition in Na_4C_{60}. *Phys Rev B* **1998**, *58*, 5-7.
44. Yoshida, A.; Okuyama, T.; Terada, T.; Naito, S., Reversible Hydrogen Storage/Release Phenomena on Lithium Fulleride (Li_nC_{60}) and Their Mechanistic Investigation by Solid-State NMR Spectroscopy. *J Mater Chem* **2011**, *21*, 9480-9482.
45. Ward, P. A.; Teprovich, J. A.; Compton, R. N.; Schwartz, V.; Veith, G. M.; Zidan, R., Evaluation of the Physi- and Chemisorption of Hydrogen in Alkali (Na, Li) Doped Fullerenes. *Int J Hydrogen Energ* **2015**, *40*, 2710-2716.
46. Teprovich, J. A.; Weeks, J. A.; Ward, P. A.; Washington, A. L.; Zidan, R., Fine-Tuning the Fluorescent Properties of Li and Na Intercalated C_{60} with Hydrogen. *Int J Hydrogen Energ* **2017**, *42*, 22511-22517.
47. Hauback, B. C.; Fjellvåg, H.; Steinsvoll, O.; Johansson, K.; Buset, O. T.; Jørgensen, J., The High Resolution Powder Neutron Diffractometer PUS at the JEEP II Reactor at Kjeller in Norway. *J Neutron Res* **2000**, *8*, 215-232.
48. Rodriguez-Carvajal, J., Recent Advances in Magnetic Structure Determination by Neutron Powder Diffraction. *Physica B* **1993**, *192*, 55-69.
49. Abdala, P. M.; Mauroy, H.; van Beek, W., A Large-Area CMOS Detector for High-Energy Synchrotron Powder Diffraction and Total Scattering Experiments. *J Appl Crystallogr* **2014**, *47*, 449-457.
50. Dyadkin, V.; Pattison, P.; Dmitriev, V.; Chernyshov, D., A New Multipurpose Diffractometer PILATUS@SNBL. *J Synchrotron Radiat* **2016**, *23*, 825-829.
51. Heiney, P. A.; Fischer, J. E.; Mcghie, A. R.; Romanow, W. J.; Denenstein, A. M.; Mccauley, J. P.; Smith, A. B.; Cox, D. E., Orientational Ordering Transition in Solid C_{60}. *Phys Rev Lett* **1991**, *66*, 2911-2914.
52. Bürgi, H. B.; Blanc, E.; Schwarzenbach, D.; Liu, S.; Lu, Y. j.; Kappes Manfred, M.; Ibers James, A., The Structure of C_{60}: Orientational Disorder in the Low-Temperature Modification of C_{60}. *Angew Chem Int Ed* **1992**, *31*, 640-643.
53. Zhou, O.; Cox, D. E., Structures of C_{60} Intercalation Compounds. *J Phys Chem Solids* **1992**, *53*, 1373-1390.
54. Beaucage, G., Approximations Leading to a Unified Exponential Power-Law Approach To Small-Angle Scattering. *J Appl Crystallogr* **1995**, *28*, 717-728.
55. Beaucage, G.; Kammler, H. K.; Pratsinis, S. E., Particle Size Sistributions from Small-Angle Scattering Using Global Scattering Functions. *J Appl Crystallogr* **2004**, *37*, 523-535.
56. Allen, A. J., Characterization of Ceramics by X-Ray and Neutron Small-Angle Scattering. *J Am Ceram Soc* **2005**, *88*, 1367-1381.

TOC Graphic